WPEDU-PR(18) 21367

P Rindt et al.

Using 3D-printed tungsten to optimize liquid metal divertor targets for flow and thermal stresses.

Preprint of Paper to be submitted for publication in
Nuclear Fusion

This work has been carried out within the framework of the EUROfusion Consortium and has received funding from the Euratom research and training programme 2014-2018 under grant agreement No 633053. The views and opinions expressed herein do not necessarily reflect those of the European Commission.

Using 3D-printed tungsten to optimize liquid metal divertor targets for flow and thermal stresses.

P. Rindt[a], J. Mata González[b], P. Hoogerhuis[c], P. van den Bosch[c], M. van Maris[d], D. Terentyev[e], C. Yin[e], M. Wirtz[f], N. J. Lopes Cardozo[a], J. A. W. van Dommelen[d], T. W. Morgan[g]

[a]Eindhoven University of Technology, Science and Technology of Nuclear Fusion Group, Eindhoven, The Netherlands
[b]Universitat Politéchnica de Catalunya, Carrer de Jordi Girona 1, 08034, Barcelona, Spain
[c]Philips Medical Systems, Veenpluis 4-6, 5684PC Best, The Netherlands
[a]Eindhoven University of Technology, section Mechanics of Materials, Eindhoven, The Netherlands
[e]SCK-CEN, Nuclear Materials Science Institute, Boeretang 200, Mol, 2400, Belgium
[f]Forschungszentrum Jülich, Institut fr Energie- und Klimaforschung, 52425 Jülich, Germany
[g]DIFFER-Dutch Institute For Fundamental Energy Research, De Zaale 20, 5612AJ Eindhoven, The Netherlands

E-mail: p.rindt@tue.nl

Abstract. Liquid metal divertors aim to provide a more robust alternative to conventional tungsten divertors. However, they still require a solid substrate to confine the liquid metal. This work proposes a novel design philosophy for liquid metal divertor targets, which allows for a two order of magnitude reduction of thermal stresses compared to the state-of-the-art monoblock designs. The main principle is based on a 3D-printed tungsten structure, which has low connectedness in the direction perpendicular to the thermal gradient, and as a result also short length scales. This allows for thermal expansion. Voids in the structure are filled with liquid lithium which can conduct heat and reduce the surface temperature via vapor shielding, further suppressing thermal stresses. To demonstrate the effectiveness of this design strategy, an existing liquid metal concept is re-designed, fabricated, and tested on the linear plasma device Magnum-PSI. The thermo-mechanical FEM analysis of the improved design matches the temperature response during the experiments, and indicates that thermal stresses are two orders of magnitude lower than in the conventional monoblock designs. The relaxation of the strength requirement allows for much larger failure margins and consequently for many new design possibilities.

Keywords: fusion, divertor, 3D-printing, tungsten, lithium, liquid metal, stress reduction, Magnum-PSI

1. Introduction

The robustness of the divertor remains a critical challenge on the way to practical fusion reactors. The plasma facing surface (PFS) must withstand $\sim$ 10 MW/m^2 for 2 full power years [1], while being eroded by the $\sim 10^{24}$ m^{-2}s^{-1} particle flux from the plasma. Meanwhile, on the millisecond timescale, transient heat loads must be expected of up to 0.5 GW/m^2 due to mitigated ELMs (30 to 60 Hz) [2, 3], or up to 80 GW/m^2 in case of an unmitigated disruption [4]. Additionally, neutron irradiation inevitably leads to material degradation [5]. Under these conditions even the state-of-the-art tungsten monoblocks [6] face a number of issues: melting [7], erosion limiting the lifetime [6, 8], and cracking of both the surface and bulk material [9]. Because of this, the monoblocks are heavily dependent on actively controlled heat load mitigation strategies [8, 10], and applicability in commercial generation fusion reactors is therefore highly reliant on the continually sustained success of such approaches, with little-to-no margin for error.

This work explores a novel design philosophy. 3D-printing of tungsten, in combination with the use of liquid metals (LM), is used to drastically reduce thermal stresses, and consequently open up many new design possibilities. Currently, tungsten produced by additive manufacturing has a reduced strength compared to traditional manufacturing, but opens up new possibilities for the use of geometries which were previously inaccessible. Philips Medical Systems specifies shape tolerances as low as ± 25 μm. This feature size is sufficiently small to enable good surface tension forces at the component surface to confine the LM. This technique can therefore be used to produce optimized porous substrates for LM based divertor targets, where the liquid serves to dissipate heat via evaporation and subsequent interaction with the plasma [11, 12, 13, 14], while simultaneously providing the thermal connection across the voids in the porous tungsten. Therefore both thermal stresses in the substrate can be minimized, while the replenishing LM flow to the PFS can be maximized.

To demonstrate this, a pre-existing LM divertor concept is re-designed for additive manufacturing. A simple concept is taken in which the plasma facing surface (PFS) is supplied passively with LM via wicking channels originating from a pre-filled internal reservoir [15]. Section 2 shows the design, and also tensile test results of the 3D-printed material. A numerical analysis of the internal stresses is discussed in section 3. Finally, the prototype is exposed to fusion relevant plasma conditions in the linear plasma device Magnum-PSI [16, 17], presented in section 4.

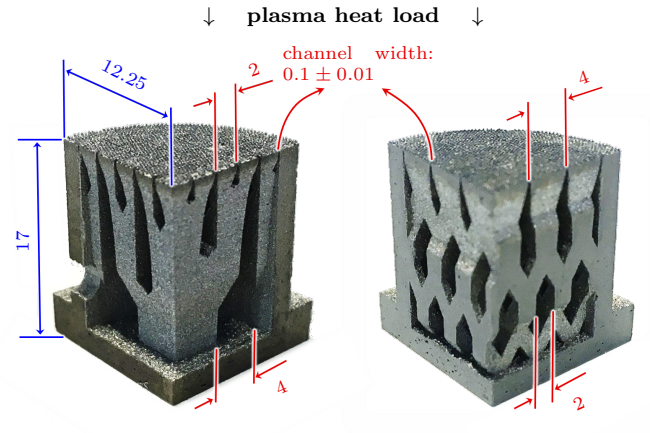

Figure 1. Quarter sections of the two resulting designs, cut by electrode discharge machining (EDM). Left: tree-type. Right: V-type. The voids serve simultaneously as both reservoir for the LM, and as wicking channel up to the PFS. At the PFS the channels are only 0.1 ± 0.01mm wide, as opposed to the 2 to 4 mm cavities at the bottom. Dimensions are in mm.

2. Design philosophy & resulting designs

2.1. Design philosophy

The above design principles were applied to the two designs presented in figure 1. 3D-printing was used to create a structure which has small dimensions in the direction perpendicular to the thermal gradient (i.e. horizontally in fig. 1). The gaps in between these structures provide room for thermal expansion, and thus thermal stresses are reduced. The same principle was used in the monoblock design, but here the dimensions have been refined more.

Filling the structure with LM allowed for thermal conduction across the gaps, and also reduced the PFS temperature via vapor shielding. In this case lithium was used because it limits the surface temperature more strongly than the main alternative, tin. However, tin can also be used in principle if a low vapour pressure LM is desired. Without LM, the 3D-printed substrate would reach much higher temperatures for a given power loading due to its high porosity and lowered overall conductivity compared to bulk tungsten. The gaps in the PFS should also be bridged by the LM, thus eliminating leading edges.

The flow that replenishes the PFS utilizes capillary action, which was first used in mesh or felt based systems [11, 18]. In this case however, the high degree of control over the printed geometry was used to maximize the flow to the PFS. Structure sizes on the PFS were minimized ($\sim$ 100 μm) to create high capillary pressure, while internal cavity sizes were maximized ($\sim$ 2 to 4 mm) to reduce drag forces and to allow for more LM to be stored.

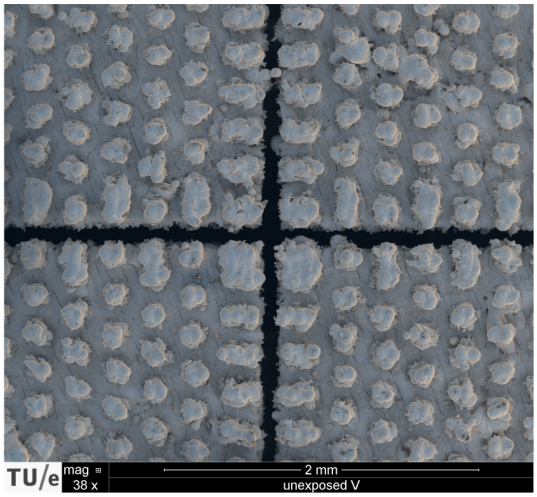

Figure 2. SEM top view of wicking channels and printed surface texturing of an unexposed V-type target. A crack network is present on the surface that is created in the printing process. Compared to an exposed target there is no observable difference. The SEM image is available in [REF].

2.2. Resulting designs

Two different target designs were made: the "tree-type" and the "V-type". The void sizes in the tree-type could be tuned by branching the solid structure and by varying its thickness. The V-type consists of a number of stacked V's, and thus the number of branches at any height is always the same. Pore sizes were only tuned by varying the material thickness. This design was intended to be more robust during handling. The pore sizes at the bottom of the tree-type target were set to 4 mm and 1.6 gram of Li could be stored in total. For the V-type this was 2 mm and 1.4 gram.

A texture was printed on the PFS to enable wicking across the surface, and stabilize the liquid surface (fig. 2). The pattern consists of dots equally spaced with $\sim$ 125 μm between them, and a height specified at 100 micron. The texture was designed to be identical for both target types. The resulting potential wicking speeds were 1.1 and 2.4 cm/s for the V- and Tree-type respectively, calculated using the expressions from [15]. The resulting thermal stresses were calculated and are presented in section 3.

The exact geometry was only constrained by the printing process itself, which allowed overhanging geometry to be printed if its angle was less than 45° or if the overhang was less than 1 mm. The outer geometry was determined by the Magnum-PSI sample holder, resulting in the top-hat shape. The circular wall and the bottom of the target serve to prevent leaking from the inner structure. The wall contains a 3 mm hole near the bottom to equalize the pressure inside and outside the reservoir.

2.3. Material strength

To assess the strength of the targets, micro tensile test samples were fabricated according to ASTM Standard E8-A356 and tested according to the ASTM D638 protocol. The samples were printed vertically, similar to the internal structures of the targets. The samples were tested without heat treatment, stress relieved (1000 °C for two hours), or recrystallized (1600 °C for one hour). Three samples were tested for each. The tests were carried out at 600 °C, which lies above the DBTT for most tungsten grades. Results are shown in fig. 3.

Although the heat treatment slightly increases the strain at which the samples fail, all samples fractured in a brittle fashion below 275 MPa. It is suspected that the crack network, visible in fig. 2, caused this behavior. The targets used for experimentation in section 4 were all stress relieved, as this resulted in the highest failure strength on average. The failure strength is significantly lower than for commonly used material grades for fusion [19], the question is if this disadvantage can be off-set by the possibility to realise low stress designs.

3. Thermal stress analysis

The thermal stresses in the component (filled with Li) were calculated using the finite element package COMSOL. An initial comparison of the two designs showed that stresses were two times lower in the tree-type target. This was not unexpected as indeed the

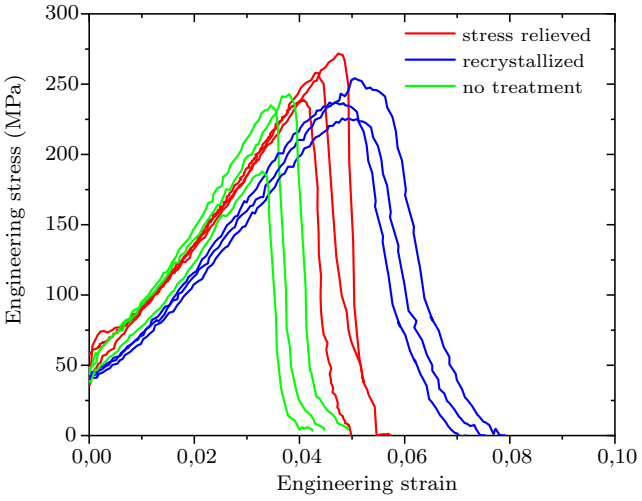

Figure 3. Tensile test results at 600 °C of samples with different heat treatments. Stress relieved at 1000 °C for two hours, recrystallized at 1600 °C for one hour, and without treatment. The samples were printed vertically, in the same orientation as the internal structures of the targets.

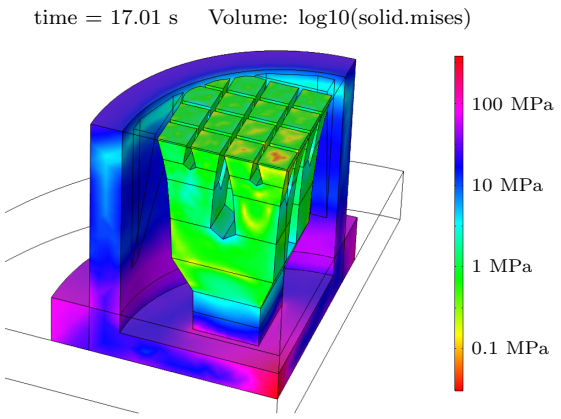

Figure 4. Von Mises stresses in the free standing tree structure are on the order 1 to 10 MPa, according to the FE simulation. A Magnum-PSI discharge is modeled consisting of a 7 s ramp-up and 10 s steady-state pulse with a peak power density of 11 MW/m^2. Dissipation via lithium vapor-shielding is included, using the model from [14]. Stresses are fairly constant throughout the discharge.

material is less interconnected in this design. As it is aimed to demonstrate the potential of this new design strategy, only the tree-type target has been considered in this section.

To mimic the plasma loading experiment from sec. 4, a 10 s pulse was applied with a peak power density of 11 MW/m^2, following a 7 s ramp-up. Heat dissipation due to the lithium is implemented according to [14]. Target holder material, clamping, and cooling were included. All details on the FEM model can be found in the replication package [REF to repository]. As shown in fig. 4, the von Mises stresses in the free standing structure were on the order of 1 MPa and did not exceed $\sim$ 10 MPa. Peak stresses occur where the branches separate, which is where the material is the widest, but also a sharp corner is present here. Details on the rendering of fig. 4 can also be found in the replication package.

Figure 6 shows the time evolution of the central surface temperature, peaking at $\sim$ 920 °C. Modeling of a target filled with LL, where vapor shielding was omitted, showed that the surface temperature would have increased to $\sim$ 1500 °C, and stresses would have increased by a factor 2. When all Li effects were omitted (thermal conduction and vapor-shielding), the melting temperature of W was approached within the exposure time, and stresses were also increased by almost an order of magnitude.

In simulations where the peak heat load was increased to 20 MW/m^2, temperatures remained below 1000 °C due to vapor shielding, consequently, also stress levels in this case were almost the same as for the case of 11 MW/m^2, fig. 4.

4. Fusion relevant plasma loading

Both target types were tested in the linear plasma device Magnum-PSI [16, 17]. A cascaded arc source in a 1.3 T magnetic field was used to create a helium plasma beam on the target with a Gaussian profile and peak power density estimated at 11 MW/m^2. The surface temperature of the exposed sample was monitored in situ via a FLIR SC7500MB IR-camera which was calibrated against a FAR SpectroPyrometer FMPI. The calibration was done on a 3 mm thick tungsten dummy target, as no pyrometer measurement could be obtained with Li. The deposited power was estimated by matching the temperature from an FEM model to IR recordings of the same dummy target. A Vision Research Phantom v12.1 high speed camera was used to view the target tangentially to the target surface.

The IR-camera view of a sample with fully wetted PFS is shown in fig. 5. Darker colors correspond to either colder surfaces or the presence of Li (lower emissivity). It was observed in-situ that lithium accumulated at the top-right edge of the sample, and also on the clamping ring. Despite this, neither the IR footage or the footage from the fast camera show signs of droplet ejection into the chamber during the 10 second main pulse.

The evolution of the central temperature and the result of the FEM are shown in fig. 6. Both display an almost flat temperature response around 900 °C. For reference, the 3 mm thin dummy target achieved a peak temperature over 1050 °C during an identical plasma

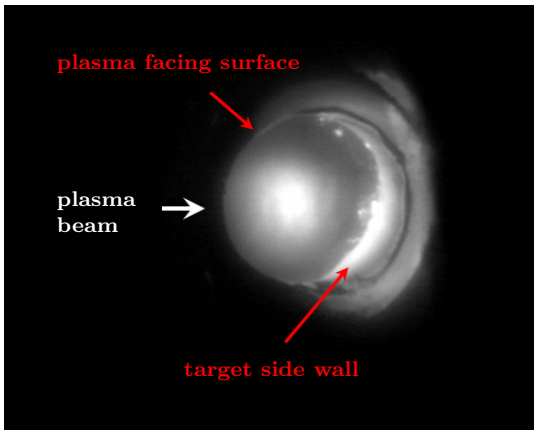

Figure 5. IR-camera view during exposure in Magnum-PSI. The beam (left) is impacting the plasma facing surface. The PFS appears to be fully wetted with Li, visible from the dark color caused by the low emissivity of Li. The side wall appears hotter (white) due the shallow viewing angle and lack of re-wetting exposing the bare tungsten. Also visible are a lithium drop at the top-right edge of the PFS, and a dark line right of the side wall indicating lithium that has wetted the base and clamping ring.

exposure, despite much more direct connection to the heat sink. Note that the steep increase and decrease in the camera signal at 7 and 17 s was merely when the target enters and leaves the camera view.

After plasma exposure, it was checked whether any damage has occurred. SEM images were taken of the PFS and of the internal structures after sectioning, for both an exposed target (cleaned) and an unexposed target. No evidence of damage was found. However, this was deemed inconclusive due to the low number of exposures.

5. Discussion

A liquid metal divertor target has been re-designed for 3D-printing according to a novel design strategy, and subsequently experimentally tested, and analyzed using a thermo-mechanical FEM simulation.

The simulation shows that peak von Mises stresses in the tree-type target lie more than a factor 20 below the failure strength. Therefore, it makes sense that no damage was observed, despite the brittleness and low failure strength of the 3D-printed tungsten. The temperature response predicted by the FEM simulation matches the experimental observations reasonably well, and can therefore indeed be used to estimate thermal stresses. It appears that both the use of mm length scales, and the presence of Li to reduce target temperature, play an important role in the stress reduction.

The thermal stresses lie 2 orders of magnitude below the stress levels encountered in the ITER monoblocks [20]. However, the 3D-printed prototypes are not yet at the same technological readiness level. For now, the best comparison is made when the peak heat load in the simulation is increased to 20 MW/m^2. In that case the Li vapor shielding causes temperatures to still remain below 1000 °C and stresses remain at a similar level.

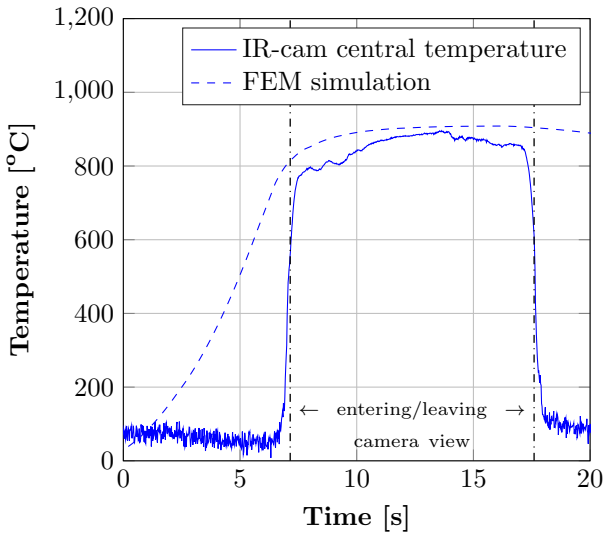

Figure 6. Central temperature on the PFS of the tree-type target from the IR recording and from the FEM simulation (dashed). Both indicate a reasonably steady temperature of around 900 °C is reached. Note that the steep increase and decrease in the camera signal around 7 and 17 s is merely when the target enters and leaves the camera view.

It should be noted that the FEM analysis did not consider the micro structure. The crack network created in the printing process (fig. 2) is suspected to be responsible for the observed brittle failure behavior in the tensile tests. Especially in the case of high pulse numbers, growth of these cracks must be expected due to stress concentration around the tips of these cracks.

The printed structure was found to function well as a Li substrate. The potential wicking speed calculated in sec. 2 is increased 20 to 50 fold compared to the wicking speed of $\sim$ 0.5 mm/s estimated for the conventionally manufactured design in [15]. In the experiment, the PFS was effectively replenished with Li and stayed wetted at all times, as observed qualitatively from the IR footage, and from the strongly reduced surface temperature.

Ejection of droplets into the plasma beam was not observed during the main pulse. This is attributed to the stabilizing effect of the surface texturing. This agrees with recent literature where texture size scales required for stability are predicted [21, 12].

Compared to mesh based systems, the PFS used here is more stable. Thermal expansion and and subsequent loss of mechanical stability as reported in [18] and observed more recently in [22], is problematic for mesh systems, especially for application to large flat surfaces. This is not an issue here.

All things considered, the ability to lower the bulk stresses is promising. As strength is no longer a critical requirement, materials with otherwise more favorable properties can be selected (e.g less prone to cracking during printing, as attempted to fabricate in [23, 24]). Additionally, the difference of at least 200 MPa between the stresses in the target and the failure strength, provides a large margin for material degradation during the lifetime of the component.

When looking ahead to a fully functional LM divertor, also a coolant channel must be considered (e.g. as suggested in [25, 12]). The stresses in the coolant channel in monoblock designs are caused to a large degree by a mismatch in thermal expansion coefficient between the CuCrZr channel and the tungsten armor. In a LM divertor other materials than pure CuCrZr may be used, due to e.g. chemical compatibilty issues with the LM. But in principle, using a 3D-printed structure filled with LM for the armor, will allow a reduction of this interface stress.

This is because there is a very low overall stiffness in the printed structure due to the low connectedness of the material. The mismatch in thermal expansion coefficient is only relevant on the small area where the individual printed structures are attached to the coolant channel. Stresses in the pipe might therefore be strongly reduced.

6. Conclusion

In conclusion, we have demonstrated a novel design strategy, making use of additive manufacturing, which allowed the successful construction and testing of liquid metal divertor targets. Designs can be made where bulk stresses are on the order of only 1 MPa, with stress concentrations up to 10 MPa, two orders below stresses in ITER-like monoblocks. Synergy between the use of additive manufacturing and LM is critical to achieve this. 3D-printing provides the geometric control over the tungsten required to minimize the stresses and maximize the LM flow to the plasma facing surface. The LM on the other hand is essential for power handling.

For future work, novel design opportunities are now created. Because strength is no longer a restricting requirement, first, materials can be used that have otherwise superior properties. Second, as a large safety margin is now available, material degradation due to for example neutron damage is much less problematic. Also for actively cooled designs, a 3D-printed/LM armor is likely to induce less stresses in a coolant channel than a solid W armor, thus reducing also the demand for strength in the coolant channel.

Overall, 3D-printing of tungsten is found to be a highly flexible manufacturing technique that allows for optimization of various design parameters due to a high degree of geometric control. It can be used to produce LM components for experimental purposes with great ease (as demonstrated here), while improving the robustness compared to traditional monoblock designs. This can be extrapolated to liquid metal divertor designs for DEMO and beyond.

7. Acknowledgement

This work has been carried out within the framework of the EUROfusion Consortium and has received funding from the Euratom research and training programme 2014-2018 under grant agreement No. 633053. The views and opinions expressed herein do not necessarily reflect those of the European Commission.

References

[1] You, J. et al., Nuclear Materials and Energy **9** (2016) 171.
[2] Loarte, A. et al., ITER ELM control requirements, ELM control schemes and required R&D, in *23rd IAEA Fusion Energy Conference, Daejeon, Korea, October 11-16, 2010*, 2010.
[3] Eich, T. et al., Nuclear Materials and Energy **12** (2017) 84.
[4] Pestchanyi, S., Pitts, R., and Lehnen, M., Fusion Engineering and Design **109-111** (2016) 141.
[5] Hasegawa, A., Fukuda, M., Nogami, S., and Yabuuchi, K., Fusion Engineering and Design **89** (2014) 1568.
[6] You, J. et al., Nuclear Materials and Energy **16** (2018) 1.
[7] Pitts, R. et al., Nuclear Materials and Energy **12** (2017) 60.
[8] Kallenbach, A. et al., Plasma Physics and Controlled Fusion **55** (2013) 124041.
[9] Li, M. and You, J.-H., Fusion Engineering and Design **124** (2017) 468.
[10] Maviglia, F. et al., Fusion Engineering and Design **109-111** (2016) 1067.
[11] Mirnov, S. V. et al., Plasma Physics and Controlled Fusion **48** (2006) 821.
[12] Morgan, T. et al., Nuclear Materials and Energy **12** (2017) 210.
[13] van Eden, G. G. et al., Physical Review Letters **116** (2016) 135002.
[14] Rindt, P., Morgan, T., Jaworski, M., and Lopes Cardozo, N., Nuclear Fusion **58** (2018) 104002.
[15] Rindt, P., Lopes Cardozo, N., van Dommelen, J., Kaita, R., and Jaworski, M., Fusion Engineering and Design **112** (2016).
[16] van Eck, H. et al., Fusion Engineering and Design **82** (2007) 1878.
[17] Rapp, J. et al., Fusion Engineering and Design **85** (2010) 1455.
[18] Lyublinski, I. E., Vertkov, A. V., and Evtikhin, V. A., Plasma Devices and Operations **17** (2009) 265.
[19] Yin, C. et al., International Journal of Refractory Metals and Hard Materials **75** (2018) 153.
[20] Hirai, T. et al., Nuclear Materials and Energy **9** (2016) 616.
[21] Jaworski, M. A. et al., Nuclear Fusion **53** (2013) 83032.
[22] Rindt, P., Morgan, T., van Eden, G., Jaworski, M., and Lopes Cardozo, N., manuscript submitted for publication to Nuclear Fusion (2018).
[23] Gu, D., Dai, D., Chen, W., and Chen, H., Journal of Manufacturing Science and Engineering **138** (2016) 081003.
[24] Iveković, A. et al., International Journal of Refractory Metals and Hard Materials **72** (2018) 27.
[25] Coenen, J. W. et al., Physica Scripta **T159** (2014) 014037.